Geophys. J. Int. (XXXX) **XXX,** XXX–XXX

The dynamics of subduction and trench migration for viscosity stratification

Alwina Enns[1⋆], Thorsten W. Becker[2†], and Harro Schmeling[1]

[1]*Institute of Meteorology and Geophysics, J. W. Goethe University,*

Feldbergstr. 47, 60323 Frankfurt am Main, Germany

[2]*Cecil H. and Ida M. Green Institute of Geophysics and Planetary Physics,*

Scripps Institution of Oceanography, University of California, San Diego, 9500 Gilman Drive, La Jolla CA 92093,

Revised version, Oct 21st, 2004

SUMMARY

Although subduction plays a dominant role for plate tectonics, related processes such as trench migration are not well understood. We investigate the influence of viscosity stratification and different flow boundary conditions on the trench migration dynamics of a subducting lithosphere in a two-dimensional model using a finite difference code. Subduction and mantle flow are driven by a compositionally prescribed density contrast between the high viscosity slab and the ambient mantle; no overriding plate is assumed. The model rheology is visco-plastic at shallow, and viscous at greater depth; the mantle is stratified with a higher viscosity in the lower part of the computational domain. The plastic rheology allows the plate to decouple from the top of the box and is described by a simplified friction law to mimic the brittle deformation of the shallow lithosphere. The flow patterns and slab morphologies differ as a function of the velocity boundary conditions (BCs). For reflective BCs, we model either a plate which is fixed on the box side, or a plate that can freely move. A slab with periodic BCs is always laterally free. We find that, when the slabs interact with the highly viscous lower mantle, the reflective BCs slab is more folded than the periodic one, due to the confinement of mantle flow around

the slab. In general, the trench is observed to roll back toward the oceanic plate. For reflective BCs free slabs the trench retreat velocity deceases after the interaction with the lower mantle. In contrast, for the periodic BC free slab it is nearly constant or even increases with time if described in a reference frame fixed to the lower mantle. The periodic BC free slab exerts a force on the lower mantle, which causes a net differential flow between the upper and lower mantle. We also carried out additional experiments with different mechanical slab properties and thicknesses. Stiffer, free slabs subduct more steeply and are able to penetrate straight into the lower mantle. After penetration into the lower mantle the trench moves continent-ward. Thinner slabs deform more easily and are folded for all boundary conditions. We can generalize the rollback systematics for free slabs by normalizing trench velocities by the plate speed. Free slabs, being more representative of the west Pacific subduction zones, show large temporal variations of normalized trench velocities ranging between a retreat value of 1.0 to an advancing value of -0.3.

Key words:

subduction – slab rollback – viscosity stratification – flow boundary conditions

1 INTRODUCTION

From first principles of plate tectonics it follows that subduction zones and trenches are no stationary features, but they migrate with respect to an absolute reference frame such as the hotspot reference frame (*e.g.* Garfunkel *et al.* 1986). In fact, the opening of oceans surrounded by passive margins requires a net closure of oceans bounded by subduction zones being associated with a net trench rollback. Until the early 1990s trench migration velocities have been inferred from evaluation of the kinematics of global plate motions. Using simplified assumptions such as vertical downwelling at subduction zones, the horizontal migration of trenches at subduction zones has been related to the dip angle of subduction. The problem with these early models was that many subduction zones are not fixed at continental plate margins, but instead are separated from these

⋆enns@geophysik.uni-frankfurt.de

†now at Department of Earth Sciences, University of Southern California, Los Angeles CA 90089-0740, USA

by back-arc basins. Due to uncertainties in the extension rates of these back-arc basins trench migration rates have been uncertain. In the last years this situation has changed dramatically due to direct GPS measurements. For example, Bevis *et al.* (1995) observed very fast extension of the Lau Basin (back-arc basin of the Tonga subduction zone), implying trench migration velocities of up to 16 cm/yr. Also in other Pacific subduction regions GPS campaigns now allow to quantify the rollback effect and back-arc spreading directly. Kato *et al.* (1998) inferred trench migration velocities of 4.4 and 5 cm/yr for the Ryukyu- and Mariana subduction zones, respectively. From GPS-measurements in the Andean region (Sella *et al.* 2002) one can estimate trench migration velocities of the Andean trench of the order of 1 cm/yr. Another region of pronounced trench rollback is the Mediterranean: tectonic reconstructions and GPS measurements suggest trench rollback of the Calabria trench during the last 38 Myr with a peak rate of 12 cm/yr and recent migration velocity of 5 to 6 cm/yr (geologic indicators) or about 0 cm/yr (GPS), and of the Hellenic trench during the last 18 Myr with a rate of 3 to 5 cm/yr (Heidbach 1999, and references therein; McClusky *et al.* 2000; Faccenna *et al.* 2003, and references therein).

The causes and the physics of trench motion are not well understood. Geodynamic modelling attempts can be divided into two categories: (1), those which prescribe the trench migration kinematics, and, (2), those with dynamically free trench migration (but sometimes with kinematically prescribed plate velocities).

Prescribed trench migration models. The first set of models has been used to investigate the relation between trench migration, slab deformation and slab penetration into the lower mantle. Christensen (1996) introduced an elegant concept of modelling subduction of a cold and highly viscous slab into a viscous mantle by prescribing a high temperature surface boundary condition on the overriding side of the subduction zone. This method effectively decouples the subducting slab from the overriding region, and guarantees contiguity of the slab within the shallow subduction zone. A different approach has been used by Olbertz *et al.* (1997), who assumed a smooth kinematic transition between subducting slab and overriding lithosphere. In the laboratory models of Griffiths *et al.* (1995), the subduction process was induced by feeding a highly viscous "slab fluid" directly into the laterally moving "mantle fluid". From all these approaches it turned out that

the resulting dip angle in the upper mantle strongly depends on the prescribed trench migration velocity, that higher migration velocities lead to slab flattening near the 660 km discontinuity (as observed in seismic tomography for some cases), and that slab penetration into the highly viscous lower mantle is delayed for fast trench migration velocities. The question arises whether in nature these effects are causes or consequences of trench migration.

Free trench migration models. In the majority of the laboratory and numerical models of Becker *et al.* (1999a) convergence velocities of the subducting and overriding plates were kinematically prescribed, while the trench evolved dynamically self-consistently. Becker *et al.* observe that trench migration may be oceanward or continent-ward depending on the buoyancy contrast between the slab and the mantle. With these models questions arise how strong the results are influenced by the prescribed kinematic side boundary conditions which control the horizontal forces in the slab. In a more self-consistent way, Zhong and Gurnis have modelled subduction as part of a large scale mantle convection flow, using a special fault formulation to dynamically decouple the subducting slab from the overriding plate (Zhong & Gurnis 1995a,b; Han & Gurnis 1999; Gurnis *et al.* 2000). They obtain a fast trench rollback effect during the early stages of subduction as long as the slab encounters the high resistance of the 660 km phase boundary and the highly viscous lower mantle. Upon penetrating into the lower mantle, trench migration slows down. Zhong & Gurnis used large models with free oceanic plates of 10000 km length. Whether their results may be applicable to smaller plates and/or plates with old continents (such as the Mediterranean cases) remains to be investigated.

Free trench migration has also been observed in the subduction models of Tetzlaff & Schmeling (2000). They modelled self-consistent subduction of a non-Newtonian slab utilizing the "hot overriding mantle - method" (Christensen 1996, see above) and focused on the kinetics of the olivine, spinel and perovskite phase transitions. Due to the increased resistance at the 660 km discontinuity trench rollback has been observed, which depends linearly on the age of the subducting slab. Furthermore, a slight increase in migration velocity occurs due to the presence of metastable olivine for old slabs. The modelled migration velocities agree well with the classical values determined by Garfunkel *et al.* (1986). However, the observed migration velocities of the Tonga and

the Calabria trenches seem to be significantly higher, suggesting other mechanisms to be responsible. The question arises of how much is the trench migration influenced by the symmetric side boundary conditions of these models.

Funiciello *et al.* (2003b) carried out numerical models of retreating slabs with visco-elasto-plastic rheology predicting dip angles and retreat velocities. However, mantle forces which act on the downgoing slab were mimicked by dashpots, neglecting viscous stresses and dynamic pressures. A thorough series of 3D laboratory experiments of retreating slabs was carried out by Funiciello *et al.* (2003a). They identify several stages of subduction, most importantly the free-fall stage of the slab sinking through the upper mantle, and a later steady-state as the slab sinks into the lower mantle. During the free-fall stage, the retreat velocity increases exponentially until it becomes constant after slab interaction with the lower mantle. Interestingly, Funiciello (2002) point out the importance of laterally free versus closed boundary conditions (at the sides perpendicular to the trench) allowing for 3D flow of mantle material around the slab. This significantly increases the magnitude of the retreat velocity. As their slabs are fixed to the non-subducting side of the model, any subduction of the (non-stretching) slab has to result in trench retreat due to geometric reasons. Thus, the modelled trench migration velocities are identical to the relative velocity of the slab approaching the subduction zone. It thus remains to be investigated how non-fixed slabs behave and whether trench migration velocities are smaller.

In the following we present a series of 2D numerical models of subduction focusing on the trench retreat as the slab sinks through the upper mantle and subsequently interacts with the highly viscous lower mantle. We first address the question of the decoupling mechanism from the overriding medium at the trench. We then focus on the importance of different boundary conditions and compare cases with symmetric (*i.e.* closed) and periodic (*i.e.* open) boundary conditions as well as laterally free versus fixed slabs. Then the effect of slab properties on the retreat velocity will be addressed. One of our major findings, a net differential velocity between upper and lower mantle (*e.g.* Davies 1999), leads to the question of the appropriate choice of reference frame. We also find that slab folding within the lower mantle strongly depends on the degree of flow constraints and slab properties.

2 MODEL AND METHOD

Our goal is to understand the dynamics of slab rollback and the interaction of the subducting lithosphere with mantle currents in a mantle with stratified viscosity. To isolate these effects, we model only the sinking oceanic and not the overriding plate (Christensen 1996). Under the Boussinesq approximation, mantle convection in the infinite Prandtl number limit can be described by the continuity equation

$$\nabla \cdot \vec{v} = 0 \tag{1}$$

with velocity, $\vec{v}$, and the conservation of momentum equation

$$-\nabla p + \nabla \cdot \tau + \Delta\rho \vec{g} = 0. \tag{2}$$

Here, τ, p, and $\vec{g}$ denote the deviatoric stress tensor, dynamic pressure, and gravitational acceleration, respectively. We will neglect thermal effects and not solve the energy equation but assign a single density contrast, $\Delta\rho|_{\text{slab}}$, between the slab and the surrounding mantle. We choose a visco-plastic rheology for the whole model domain such that

$$\tau = 2\eta_{\text{eff}}\dot{\varepsilon} \tag{3}$$

where $\dot{\varepsilon}$ is the strain rate tensor. The effective viscosity, η_{eff}, is defined by a Newtonian and a plastic term as

$$\frac{1}{\eta_{\text{eff}}} = \frac{1}{\eta_{\text{N}}} + \frac{1}{\eta_{\text{yield}}} \tag{4}$$

where

$$\eta_{\text{yield}} = \frac{\tau_{\text{yield}}}{2\dot{\varepsilon}_{II}} \tag{5}$$

with $\dot{\varepsilon}_{II}$ as second invariant of the shear strain rate (see also Schott & Schmeling 1998). Material yields plastically if the second (shear stress) invariant of τ, τ_{II}, reaches a critical τ_{yield}. This behavior is approximated by determining η_{yield} such that $\tau_{\text{II}} < \tau_{\text{yield}}$ at all times. To mimic the brittle behavior of a fault-filled crust τ_{yield} is calculated from a Coulomb friction law for optimally oriented faults

$$\tau_{\text{yield}} = (a\sigma_n + b)\,\lambda \tag{6}$$

with a and b denoting constants, σ_n for the normal stress, and the pore pressure factor

$$\lambda = 1 - \frac{p_{\text{pore}}}{p_{\text{lith}}}, \tag{7}$$

which describes the fluid pore pressure, p_{pore}, of the lithosphere relative to the lithostatic pressure

$$p_{\text{lith}} = \rho g z. \tag{8}$$

Here, z denotes depth and g the magnitude of $\vec{g}$. The λ factor is poorly constrained in nature and used as a constant, adjustable parameter for slab weakening in our models (sec. 3.1). For simplicity we assume $\sigma_n = p_{\text{lith}}$.

The viscosity of the slab, $\eta_{\text{N}}^{\text{slab}}$, is always set to a constant multiple of the upper mantle viscosity to approximate mechanical differences between subducting plate and mantle which are of thermal and chemical origin in nature. The mantle viscosity jumps from its reference value in the upper mantle, $\eta_{\text{N}}^{\text{um}}$, to a higher value, $\eta_{\text{N}}^{\text{lm}}$, in the lower mantle. In this way, we capture the effect of an increase in viscosity in the lower mantle which is well documented and commonly associated with the 660 km phase transition (*e.g.* Hager 1984; Mitrovica & Forte 1997). However, we neglect possible other effects of phase transitions, for instance those related to a negative Clapeyron slope of the ringwoodite $\rightarrow$ perovskite + magnesiowüstite transition (*e.g.* Christensen 1996; Tetzlaff & Schmeling 2000). Table 1 lists all parameters and the value (ranges) we have used in our models.

We solve eqs. (1) and (2) in two dimensions using a stream function approach. The finite difference (FD) code `FDCON` by Schmeling & Marquart (1991) is used with a resolution of 101×301 grid-points for a model geometry (Fig. 1) with aspect ratio 1×3 spanning a depth–width range of 1320×3960 km. Compositional differences between slab and mantle are treated by a tracer advection method; we use 800×2400 markers, which are initially roughly evenly distributed. Model results were found to be stable with respect to increasing resolution, both in terms of FD grid and marker number.

Mechanical conditions are free-slip, impermeable on the top and bottom boundaries. Side boundaries are either treated as reflective (free-slip) or periodic (*e.g.* Gottschaldt 1997) to explore the effect of constrained mantle flow (sec. 3.2). In all models, the stream function was set to a constant, zero value at the top and bottom implying zero net horizontal flow. Thus, our box

reference frame, which we used for calculations, corresponds to center of mass reference frame by Han & Gurnis (1999). To obtain a net horizontal flow in the box, one could add a constant horizontal velocity to the whole model. This would lead to an identical solution of the momentum equation.

The initial slab configuration was prescribed asymmetrically to facilitate the development of subduction on the one side of the plate as shown in Fig. 1. The oceanic plate away from the trench was detached from the side boundaries ("free slab") for all periodic boundary conditions (BCs) models. For reflective boundary conditions the oceanic plate away from the trench was either detached from the side boundaries or it was attached to the side wall ("fixed slab"). We note that periodic free slabs cannot be pinned in this fashion because this would imply over-constrained mechanical BCs, namely fixing one particular point of the slab to the net horizontal velocity of the whole model. Thus, all periodic BCs models have a free slab.

3 RESULTS

3.1 The trench decoupling mechanism

Before discussing the time-dependence of subduction and trench motion for different boundary conditions, we now explore the role of the plastic, "Byerlee", yielding. For viscous flow models, it is difficult to initiate and obtain slab-shaped downwellings without describing a trench-geometry (*e.g.* King & Hager 1990; Conrad & Hager 1999) or surface velocities (*e.g.* Christensen 1996). To avoid having Rayleigh-Taylor instability-dominated, blob-type slabs, we choose to augment a purely viscous rheology with yielding in an attempt to mimic faulting in the brittle deformation regime of the uppermost lithosphere (eq. 4). Depending on the yielding parameters, there are large differences in the slab shapes and the time needed for the downwellings to reach mid mantle depths. Fig. 2 shows models at roughly the same state of subduction for different choices of the pore pressure factor λ.

The maximum depth of the slab versus time is shown in Fig. 3 to illustrate the time-dependence of the downwelling flow that is associated with the models shown in Fig. 2. For the dry, $\lambda = 1$, case a Rayleigh-Taylor instability forms and the dense material sinks slowly into the mantle while

thinning at mid upper mantle depths, indicating a resistance of the uppermost slab material to detach from the free-slip surface.

The sinking velocities as indicated by Fig. 3 are slower for $\lambda = 1$ than for the weak yielding case of $\lambda = 0.1$. These differences are caused by changes in the effective slab viscosity (eq. (4)), which is unaltered in the bending region but slightly lower at the trench with $\sim 70 \cdot \eta_N^{um}$ for $\lambda = 1$. The $\lambda = 0.1$ case is characterized by a well-defined slab, little intra-slab deformation. The bending region of the slab attains an effective viscosity of $\sim 50 \cdot \eta_N^{um}$, with a minimum of $\sim 10 \cdot \eta_N^{um}$ at the decoupling zone. The viscosity of the plate part, which is not subducted, is reduced on the surface to $\sim 80 \cdot \eta_N^{um}$ for depths of $z <\sim 20$ km. The subducted part of the slab is not weakened for $z >\sim 200$ km.

In contrast, $\lambda = 0.01$ leads to a strong weakening and slab thinning in the trench region with eventual slab tear-off at the surface. Viscosities at the trench are lower than those of the upper mantle ($\sim 0.05 \cdot \eta_N^{um}$). The stiffness of the bending region is strongly reduced to $\sim 30 \cdot \eta_N^{um}$ during the initial subduction stage before slab tearing. The subduction velocity is moderately faster than for larger λ values (Fig. 3), indicating a strong control of the weakening mechanism at the trench which would be enforced by power-law rheology.

From this comparison of different Byerlee strengths, we choose $\lambda = 0.1$ for the models below, since the slab detaches freely from the surface and roughly retains its thickness without necking. The choice of $a \cdot \lambda$ is consistent with the range of values for the friction coefficient, which could be applicable to the subduction zones on Earth, given *e.g.* by Moresi & Solomatov (1998). Without a brittle lithosphere or with high values of $a \cdot \lambda$ Moresi & Solomatov (1998) did not observe mobile lid convection in their models. Furthermore, in the numerical experiments of Schott & Schmeling (1998) delamination and detachment of the mantle lithosphere occurred only if the lithosphere was weakened. Reasonable sinking velocities of the lithospheric root were obtained for λ values of $\sim$0.07. In accordance with these models, the weakening of the lithosphere in our experiments is necessary to detach the slab from the surface and to allow the plate to move freely. Varying other parameters at fixed a, b and λ, we expect that the dynamics of subduction will be controlled

by viscous slab bending and the interaction of the slab with mantle flow in a stratified viscosity setting, and not the upper boundary condition (*cf.* Funiciello *et al.* 2003a).

3.2 Stratified mantle subduction: Influence of boundary conditions

Fig. 4 shows the development of subduction for our reference model with $\lambda = 0.1$, slab thickness of $d = 99$ km and stiffness of $\eta_N^{slab} = 100\eta_N^m$ for three different settings: free slab for periodic and reflective BCs, and fixed slab for reflective BCs. The natural analog for these different end-member settings would be an oceanic plate which is relatively short and weakly coupled to a ridge, with flow determined by the plate alone (Fig. 4a) or with restricted flow, possibly due to neighboring subduction zones or large-scale convective currents (Fig. 4b). Fig. 4(c) would correspond to subduction on the side of a plate which is relatively large and slowly moving, such as slabs in the central Mediterranean attached to the African plate. For (c), all subduction has to be taken up by in-slab deformation and rollback.

The time-dependence of several subduction features for the models shown in Fig. 4 are compared in Fig. 5.

3.2.1 Slab folding

We can distinguish different slab morphologies and flow patterns due to the interaction of the sinking slab with the 660 km viscosity contrast. All models show slab flattening and a reduction in the subduction velocity once the slab notices the viscous drag effect of the lower mantle during its descend (at $t \sim 5.5$ Myr). Part of the subduction motion is always taken up by oceanward trench rollback; in the case of the fixed slab (Fig. 4c), this is simply a consequence of conservation of mass. Note also that the free slab model shows the development of a second downwelling to the right of the subducting plate as a viscous instability for times larger than $t \sim 12$ Myr (Figs 4a and b).

We observe folding of the slab at depth, an effect that is most pronounced for the reflective free slab (Fig. 4b), but also is a prominent feature of the fixed slab (Fig. 4c). For periodic BCs no folding is observed (Fig. 4a). The basic difference between periodic and reflective side boundaries

is that the descending slab can introduce a relative current in the lower mantle and "push" material to the side for periodic BCs. Thus the periodic BCs increase the horizontal mobility of the lower mantle and allow lateral movement of the trench relative to the position of the slab material, which slowly penetrates into the lower mantle with the result of no folding (Fig. 4a). If, due to lateral confinement of mantle material at the box sides, the trench position overlies the point of lower mantle penetration for some time as in Fig. 4(b), the difference between upper and lower mantle subduction velocities results in folding. This condition is still met in the fixed slab case, as can be verified by inspecting Fig. 4(c). Indeed, combining Fig. 5(b) and (c) reveals that the folding cases are characterized by slow trench retreat velocities relative to the lower mantle, while the non-folding case has a higher (3 – 4 cm/yr) retreat velocity at the late stages. This finding is corroborated by additional experiments we performed for a fixed slab with reflective BCs and larger aspect ratios (not shown). There, folding is also reduced compared to the smaller aspect ratio models since a larger aspect ratio slab allows a larger differential velocity between trench and lower mantle.

Slab folding can be understood as a viscous instability whose growth rate depends on the viscosities of the mantle and plate, the plate thickness and the layer (or slab) parallel compressive force (*e.g.* Turcotte & Schubert 1982, p. 262). For a sinking slab that encounters a viscosity contrast, the slab parallel compression is higher for a vertical than for an inclined slab, because the latter can "push" the lower mantle material to the side. Therefore, there is no folding if the subduction velocity contains a significant component parallel to the mobility of the lower mantle, and/or if the viscosity and thickness of the slab are large. An increased lower mantle viscosity decreases its mobility, raises the slab parallel compressive force, and hence leads to larger folding tendency.

3.2.2 Interaction with 660 km and rollback

From the maximum depth of the slab, $z_{\mathrm{slab}}(t)$, in Fig. 5(a), we can observe two stages of subduction, before and after the effect of the 660 km and sluggish lower mantle flow is felt by the downwelling (*cf.* Funiciello *et al.* 2003a, and compare our Fig. 3). Differences in $z_{\mathrm{slab}}(t)$ between

BCs for the free slab setting are small, while the fixed slab descends at slightly smaller speeds. Absolute values of subduction velocities are of the order of ~ 10 cm/yr. We discuss how the time-dependence of subduction might be influenced by neglected mechanisms which were not included in our models in sec. 4.1.

The second stage of subduction is near to steady-state and characterized by roughly constant subduction and plate velocities (Figs 5a and d), in contrast to acceleration of the slabs in the upper mantle.

A greater difference for the three initial and boundary condition settings is displayed by the trench velocities, shown in the box reference frame in Fig. 5(b). For reflective boundary conditions, oceanward rollback is steady initially and then reduced substantially once the slab comes close to 660 km, where escape flow has to be increasingly channeled through the stiffer lower mantle.

As expected at least for the initial stage the fixed slab model has larger rollback velocities than the free models. However, the ponding of the fixed slab on the 660 km boundary leads to flow confinement and folding of the slab, which strongly slows down the trench retreat. The initially faster rollback rates of the fixed slab become slower than the rollback speeds of the periodic free slab at ~ 6 Myr. The flow confinement imposes a rather strong constraint so that the rollback velocity of the fixed slab becomes significantly smaller than the subduction velocity (compare Figs 5a and b). This can only be accomplished by significant stretching of the lithosphere and slab (*cf.* Fig. 4c versus Figs 4a and b).

The model with periodic BCs displays slow retreat throughout the model run (Fig. 5b), without much rate variations and no clear effect of the 660 km viscosity jump. This can be attributed to the ability of the slab to induce a net flow in the lower mantle (Fig. 4).

3.3 Influence of slab properties

3.3.1 Stiff slab

To illustrate the effect of a stiffer slab with $\eta_N^{slab} = 500\eta_N^m$, we show additional model snapshots in Fig. 6 and the corresponding time-dependence of model parameters in Fig. 7. Subduction is slower than for the reference model of Fig. 4, and the slab reaches 660 km at ~ 8 Myr, roughly 2 Myr

later than for $\eta_N^{slab} = 100\eta_N^m$ (Fig. 7a). The viscous bending of the slab at the trench dominates the models initially and causes a lower speed of subduction (*cf.* early stages of Figs 5a and 7a). In addition to the slab morphologies which are different for the ponding stage, we therefore also find a dependence of subduction velocities on slab viscosity during the first stage of slab descent. This difference is, however, not as large as in the case of slab viscosity being the only control of subduction (Becker *et al.* 1999a; Funiciello *et al.* 2003a,b), indicating an important effect of mantle currents already at the early stages of subduction. Once the bending is overcome and subduction fully developed, the mantle drag appears to dominate, and the peak of the subduction velocity is only slightly lower than for smaller slab viscosity. (Figs 5a and 7a, 5 – 10 Myr).

On the one hand, the folding tendency for all BCs cases is reduced in the sense that undulations in Fig. 6 are of longer wavelength and slower folding growth rates than in the reference slab in Fig. 4, consistent with a viscous instability. Accordingly, we also do not see the development of a Rayleigh-Taylor type de-blobbing on the left plate edge as was found in Fig. 4(a), (b) for the stiff slab during the model run. On the other hand, stiff slabs for Fig. 6(a) penetrate more steeply into the mantle (*cf.* Davies 1995) and are not slowed down by the lower mantle as much. The subduction velocity of the deepest part of the slab after slab penetration into the lower mantle reduces to about a half of its maximum value compared to $\sim$ a quarter of the maximum velocity value for the reference slab (Figs 5a and 7a). The steep subduction leads to two well defined convection cells around the slab, comparable to the reflective boundary condition case of Fig. 4(b). Accordingly, the folding tendency increases in the periodic free slab in Fig. 6(a), and some undulations in the retreat, lower mantle and plate velocities are visible in Figs 7(b), (c), (d), respectively. The fixed slab does not show any folding instability any more (Fig. 6c). This is due to the reduced lithosphere stretching compared to the reference model (Fig. 5d), displacing the trench from the position of lower mantle penetration.

The different trench motion behaviour depends on how the slab transmits forces and momentum to the lower mantle. Stages of pushing the lower mantle relatively forward and backward alternate (Fig. 7c), and the backward bending, more common for stiff slabs, is related to continent-ward trench motion. Compared to the reference slab, the free stiff slabs have always slower oceanward

trench retreat velocities than the fixed stiff slab. As Fig. 7(c) shows, the initially steeper descent for the stiff slab (compare Figs 6a and b) leads to more similar lower mantle currents for periodic and reflective BCs, implying that the slab is not able to exert a significant net push on the lower mantle within the first 20 Myr. Only at late stage (25 Myr) backward-bent subducting slab within the upper mantle in combination with periodic BCs (not shown) accelerates the trench to continentward velocities of over 2 cm/yr. The mechanism for the excitation of lower mantle flow is therefore dependent on slab rheology, the steepness of subduction through the upper mantle and the details of interaction with 660 km.

3.3.2 Thin slab

A thin subducting slab is shown in Figs 8 and 9, corresponding to a younger slab where the hypothetical isotherm defining the cold, oceanic lithosphere would have had less time to diffuse into the mantle. For the thin slab, the rheology contrast between slab and mantle is less important for the overall flow characteristics. Rather, the mantle flow strongly shapes the slab. This is evidenced, for instance, in the pronounced formation of a "mushroom" shape at the slab tip after interaction with the higher viscosity lower mantle; a feature commonly seen in models of sinking density anomalies in only radially stratified media (*e.g.* Kárason 2002, for a slab application). The thin slab is also more easily bent, leading to strong folding for all boundary conditions displayed in Fig. 8.

Compared to the reflective free and fixed slabs the trench retreat for the thin periodic free slab is the slowest initially and the fastest finally, as was observed for the reference models. But in contrast to the reference models the trench retreat of all thin slabs is not constant during the first 4 Myr, but increases steadily before interaction of the slab with the lower mantle (Figs 5b and 9b). There is also some increase of the trench retreat seen for the stiff slab (Figs 7b). The early stage of subduction in the models is influenced by the prescribed dipping edge of the plate at the beginning of the model run. The slab shows increasing and then constant subduction velocity until $\sim$4 Myr (Fig. 9a), which is caused by the decreasing bending radius and weakening of the bending region.

If the certain geometry and rheology of the slab are reached, the slab descent is not influenced by the initial slab shape any more.

The behaviour of the periodic and reflective free slabs is similar initially, and after the interaction with 660 km the trench retreat velocity shows stronger undulations for the reflective slabs than for periodic ones.

3.4 Relative trench migration velocity

Some systematics of the trench migration velocity can be inferred from the models when distinguishing between different subduction stages. Figs 10a and b show the trench migration velocities, v_t, normalized by the plate velocity, v_p, for the models with free slabs discussed above. We call this quantity the relative trench migration velocity (RTMV). For the fixed plate we cannot define RTMV in this manner because of the very low plate velocities.

Periodic free slabs. The early stage of subduction is characterized by an initially high RTMV (retreat velocity up to twice the plate velocity), which rapidly decreases until the slab starts to interact with the 660km boundary. As the slabs begin to penetrate into the lower mantle, increasing resistance slows down subduction velocities. As a result the relative retreat velocities increase again, reaching values as high as 0.8. At late stages, however, RMTV decrease again, probably because the surface part of the plates becomes small. Alltogether, at intermediate or late stages of subduction our periodic free slab models predict trench retreat velocities having a substantial fraction (0.4 ± 0.3) of the plate velocities.

Reflective free slabs. During the early stages of subduction, the RMTV-curves are roughly similar to the periodic free slabs and the trench migration velocitiy exceeds several times the plate velocity. However, at later stages the reflective free slabs experience stronger lateral contraints than the periodic slabs, which results in significantly smaller, almost negligable RTMVs after interaction with the 660km boundary.

4 DISCUSSION

4.1 Model limitations

Amongst the effects we have neglected in our model are, in perceived order of increasing importance, sphericity, elasticity, temperature diffusion, phase boundary effects other than viscosity increase, lateral viscosity contrasts in the mantle (possibly due to an asthenospheric channel below the oceanic plate), power-law rheology, and three-dimensional, time-dependent flow effects.

The average viscosity of a subducting plate is subject to debate. Rheological laws determined in the laboratory (*e.g.* Ranalli 1995) would predict very stiff slabs. However, many features of subduction zones can be explained with fluid models (*e.g.* Vassiliou & Hager 1988; Tao & O'Connell 1993; Zhong & Gurnis 1994), and seismically determined strain rates within slabs are comparable to the ambient mantle (Bevis 1988). This implies an effective weakening of the slab relative to a simple temperature dependent rheology (*cf.* Čížková *et al.* 2002). Furthermore, the viscosity of the subducting slab at the trench may be important in controlling slab dynamics. Models find upper limit, effective trench viscosities of the subducting plate of $\sim 10^{23}$ Pa·s (Conrad & Hager 1999; Becker *et al.* 1999a).

The effectiveness of diffusion to weaken the temperature dependent slab viscosity will depend on the local Peclet number and, while probably small, can be expected to reduce slab viscosity somewhat before slabs reach 660 km. Large bending strain-rates can lead to slab weakening in the trench region if a power-law rheology is active at shallower depths in the lower temperature mantle. Both strength-reduction effects can be expected to accelerate subduction, as is also shown by the varying yield stress models of Figs 2 and 3.

An asthenospheric lower viscosity region, which might exist under oceanic lithosphere, would furthermore speed up our subduction velocities as the amount of drag underneath the horizontal part of the plate would be reduced. Since driving forces and stresses scale only with the slab-pull density contrast $\Delta\rho|_{\text{slab}}$, model velocities are inversely proportional to $\eta_{\text{N}}^{\text{um}}$ and increase linearly with $\Delta\rho|_{\text{slab}}$. As our simplified model does not include these accelerating ingredients, we have chosen to scale it with 10^{20} Pa·s as an effective mantle viscosity (Table 1). If we use the canonical

viscosity value of 10^{21} Pa·s from post-glacial rebound for the upper mantle instead, the subduction velocities shown in Figs 5, 7, and 9 would be lower by a factor of ten.

The effect of the 410 km and 660 km phase transition, which have both been neglected in terms of the associated density changes, has been discussed extensively (*e.g.* Christensen 2001, for a review). While it is well established that the 410 km will have an accelerating effect on subduction, the effective Clapeyron slope of the 660 km might be almost zero (*e.g.* Weidner & Wang 1998), implying a small density effect. However, models that include phase change dynamics can be expected to show more episodicity in terms of rollback dynamics (*e.g.* Zhong & Gurnis 1995a).

4.2 Reference frames and net motions

While the net horizontal flow of the whole mantle has to be zero (sec. 2), there may exist a mean horizontal velocity of the lower mantle for both periodic and reflective BCs models. Only for the former case, however, does this motion correspond to a net motion of the lower mantle with respect to the lithosphere. For the latter, reflective boundary conditions one has to take into account the mirror image with velocities opposite of the box which is actually modelled. Would we average over this pair of cells, the net horizontal motion of the lower mantle would cancel out to zero. The excitation of net relative rotation motion between upper and lower mantle for periodic boundary conditions is only possible for laterally varying viscosity (Ricard *et al.* 1991; O'Connell *et al.* 1991) such as subduction of high viscosity slabs.

The comparison of the induced lower mantle currents for different slab properties (*e.g.* Figs 5 and 7) demonstrates that the slab mechanism for excitation of net relative lower mantle motion which we described above will depend on the interactions of the slab with the 660 km rheological contrast. Slab/660 km interaction induced net rotation could be invoked as an explanation for the observed net rotation in hotspot reference frame. This hypothesis should be tested with global 3-D models. The relative net rotation of the lower mantle could also be caused by the continental roots as was observed in the numerical experiments by Zhong (2001).

Since we are dealing with mean horizontal motions relative to the oceanic plate, we could define alternative reference frames for slab motions, specifically trench motion. Previously, we

viewed velocities in a box-relative framework (*e.g.* Figs 5b and 5d) which in nature would have to be defined based on neighboring convection cells. An alternative reference frame is with respect to a stable lower mantle, where we could subtract any total mean horizontal motion of the lower layer (Fig. 5c) from trench (Fig. 5b) and horizontal plate velocities (Fig. 5d) (*cf.* Garfunkel *et al.* 1986).

If we display trench migration velocities in the lower mantle and box reference frames for periodic and reflective free slabs (reference models, Fig. 11a and b), the difference between velocities in both reference frames is of the order of 10% for reflective BCs. For periodic BCs the velocity in the lower mantle reference frame is about twice as high as in the box reference frame after the slab interaction with the lower mantle.

Since we cannot incorporate the effect of other large scale currents and subduction that will affect flow in nature (*e.g.* Steinberger & O'Connell 1998), our lower mantle reference-frame would only be a regional realization of hypothetical lower mantle, hotspot reference-frame on Earth. Therefore we used the box reference frame for all models (*cf.* Han & Gurnis 1999) while taking into account that the relative trench migration velocities for periodic BCs and late subduction stage could be higher in the lower mantle reference frame.

4.3 Comparison with previous work

All of our models with stratified viscosity are characterized by a slowdown of subduction and ponding (*cf.* Gurnis & Hager 1988). If we increase the contrast between upper and lower mantle viscosity to larger values of ~ 150, the vertical motion of the slab is strongly reduced and a long ponding stage results. Our findings on the deformed slab shapes at depth are consistent with earlier work that showed that phase transition dynamics (Zhong & Gurnis 1995a; Christensen 1996) and density or viscosity layering (Kincaid & Olson 1987; Gurnis & Hager 1988; Gouillou-Frottier *et al.* 1995; Griffiths *et al.* 1995; Christensen 1996) can produce a variety of ponded slab shapes at 660 km as a function of rollback. Furthermore, Gaherty & Hager (1994) showed that compositional contrasts in the slab can lead to strong folding as well. However, we find that the various degrees of flow confinement to which two dimensional models are limited (explored by periodic and reflective BCs models) are important for determining the shape of a slab at depth (*cf.*

Faccenna *et al.* 2001a,b). The choice of periodic BCs leads also to a shallower dip angle of the slab after its interaction with the viscosity contrast as was observed by Gurnis & Hager (1988) and Han & Gurnis (1999). In our model framework, the various slab morphologies and the ponding of subducted material at or above the 660 km transition which are seen in seismic tomography (*e.g.* Fukao *et al.* 2001; Becker & Boschi 2002; Kárason 2002) would be explained as a function of the descend of dense material that interacts with a viscosity contrast, with the surface observable of various rates of trench rollback.

Amongst the effects that may determine the long-term fate of deep slab subduction, slab rollback and the effect of the phase transition are well studied (*e.g.* Christensen 2001). However, many of these models treat rollback as an input parameter (Gouillou-Frottier *et al.* 1995; Griffiths *et al.* 1995; Christensen 1996) and there are few studies which have focused specifically on the question of how trench motion results dynamically consistent from the slab dynamics (Kincaid & Olson 1987; Zhong & Gurnis 1995a), as we have striven to do here. Zhong & Gurnis's (1995) work is probably closest to our approach: for a cylindrical domain and a negative Clapeyron slope, those authors observed that slab rollback was strongest during the slab descent and the ponding phase on 660 km. Once material breaks through the phase boundary, trench motion was strongly reduced. We find a similar decrease in rollback velocities for our reflective boundary condition models where the sluggishness of flow in the lower mantle controls trench migration. However, for a certain range of slab parameters, our periodic BCs models are either not affected by 660 km (box reference frame), or show re-acceleration after transient slowdown (lower mantle reference frame). It is difficult to compare our models with Zhong & Gurnis (1995a) because we have no negative Clapeyron slope. However, the convective currents in Zhong & Gurnis's (1995) cylindrical model may be more similar to our reflective case, consistent with the interpretation that rollback will be slowed down by confined flow.

The division of subduction into two phases (initial acceleration and slowdown after the lower mantle is felt) was also discussed extensively for laboratory analog models by Faccenna *et al.* (2001b) and Funiciello *et al.* (2003a). Our numerical models for free oceanic plate subduction show behavior similar to Funiciello *et al.* (2003a) for reflective boundary conditions. Again,

boundary conditions are not exactly the same since the Funiciello *et al.* (2003a) approach has a natural no-slip condition at the side walls. The source of episodicity for rollback in the analog models was attributed to lateral, toroidal flow around the slab, which we cannot incorporate into our 2-D models.

4.4 What is the cause of rollback?

A consistent interpretation emerges from our models. If flow is confined, by lateral material contrasts due to neighboring slabs, convective cells, or restricted flow through the lower mantle in 2-D numerical experiments with reflective boundary conditions, rollback is slowed down and the trench stagnates after interaction with 660 km. If there is the possibility of escape flow, laterally or by means of periodic boundary conditions in 2-D, rollback velocities are always a substantial fraction of the plate velocity. We conjecture that the physical reason for rollback lies in the minimization of the total dissipation rate of the flow driven by the subducting slab. This dissipation is partitioned into a) a shear flow contribution that is induced by horizontal motion of the oceanic plate at the surface and b) a contribution due to the sideways moving slab that is sticking into the mantle (i.e. the rollback contribution). For a given rate of change of potential energy due to subduction it appears that the rollback mode is often energetically favorable because it reduces dissipation due to shear flow a) more than it increases dissipation due to roll back b). Quantitative tests of this suggestion will be the subject of a future study.

4.5 Application to natural subduction zones

In terms of the general behavior of subduction, our fixed slab, reflective boundary condition model (Fig. 4c) is most applicable to the central Mediterranean, where the small Calabrian slab is attached to the slowly moving, large African plate. This setting has been discussed by Faccenna *et al.* (2001a), and our models are consistent with predicting rollback for this situation at a rate about half the subduction rate. In addition to the apparent stagnation of the Calabrian slab above 660 km (*e.g.* Spakman *et al.* 1993; Piromallo & Morelli 2003), the presence of the Hellenic slab and remnant subduction makes the Mediterranean also a likely candidate for lateral flow confinement.

In the Marianas and the Tonga subduction zones, back-arc spreading is observed, and especially the Tonga trench shows rapid rollback (Bevis *et al.* 1995). This setting where the Pacific plate is moving rapidly toward the trench is more similar to our free slab cases (Figs 4a and b). There is also evidence for substantial deformation of the slab at depth (Giardini & Woodhouse 1986; van der Hilst 1995). These findings single out Tonga as a natural example for fast rollback with slab complexity at depth, possibly related to flattening and folding as observed for the periodic or reflective BCs case of our reference model (Fig. 4a or b, respectively). From these two models, only the periodic BCs case has a relatively high normalized trench migration velocity of about 0.8 (Fig. 10).

In the Sunda arc, deep seismicity within the Wadati-Benioff zone appears to denote a tendency of the subducting slab to bend over backward toward the oceanic plate at depth (*e.g.* Isacks & Barazangi 1977; Schöffel & Das 1999; Becker *et al.* 1999b). This slab behavior might indicate that the compressional deformation state of the overriding plate at the surface (*e.g.* Jarrard 1986; Letouzey *et al.* 1990; Bock *et al.* 2003) is related to slab interaction with the 660 km boundary. Slabs with advancing trenches could potentially cause compression in an overriding plate. In our experiments, continentward trench motion is mostly seen for stiff slabs and reflective BCs models and only after the slab reaches 660 km. A similar behavior with advancing slabs after forward rolling on 660 km is also seen in laboratory experiments for certain parameter ranges (Faccenna *et al.* 2003a).

Seismic tomography has been used to argue for whole mantle style convection, accompanied by ponding and a range of slab morphologies at depth. This spurred the early geodynamic models which evaluated the effect of rollback on slab penetration. However, it is not clear if there is already (or if there will be any time soon) enough resolution to delineate folding of slabs, which previous geodynamic models and this study have documented as plausible behavior in certain parameter ranges. Periodic boundary condition models, which allow for a greater amount of flow around the slab, as would be expected in the 3-D Earth in general, are less likely to show folding. We should therefore consider more simple, flat ponding as the more robust behavior of slabs which interact with a viscosity jump. Indeed, quite complex slab images such as under the Sunda arc can

plausibly be explained by the simple impingement of a weak (mantle viscosity) slab on a strong viscosity change with time-dependent trench motion (Kárason 2002).

Models that treat rollback consistently such as ours show that the shape of the slab depends quite critically on the large scale mantle flow. Besides that, slab anomalies at depth will also be affected by the change in plate boundary configurations and plate velocities with time (Lithgow-Bertelloni & Richards 1998). If slab anomalies are furthermore advected laterally by mantle flow in such subduction history reconstructions (Steinberger 2000), a better match with tomography should result. However, this is not necessarily the case at other than the largest heterogeneity length-scales (Becker & Boschi 2002). We can therefore hope that improved models with a higher degree of rheological realism (*e.g.* Tan *et al.* 2002) will be able to allow us to construct individual subduction zones with a higher degree of accuracy, assuming that tomography will be able to provide ground truth.

5 CONCLUSIONS

We find that the accelerating phase of subduction in the upper mantle leads to substantial slab rollback rates of the order of 0.5 of the plate speed. Once the high viscosity lower mantle is affecting the slab descent, the rollback is reduced or halted for reflective boundary conditions representing flow confinement. However, for periodic boundary conditions, more appropriate for isolated subduction zone on Earth, the rollback rate remains constant in time or re-accelerates after an initial slowdown. Amongst the considered boundary and initial conditions, a slab which is attached to a relatively immobile plate shows strongest rollback before the interaction with 660 km boundary, since in-slab deformation is small and mass must be conserved. It is important to reevaluate the appropriateness of 2-D models to subduction on Earth since the choice of mechanical boundary conditions turns out to be critical.

The subduction of the fixed slabs occurs due to the thinning of the lithosphere and to the trench retreat.

Oceanward movement of the trench is observed for most of the free and all fixed slabs. Only free stiff slabs are bent over backward toward the oceanic plate at depth and penetrate straight into

the lower mantle. They show continentward trench migration after the interaction with 660 km viscosity contrast.

The subduction velocities depend on the viscosity of the slab in the initial stage and reach maximum values of the same order for reflective and periodic free slabs before the penetration of the slabs into the lower mantle.

Complexities in slab morphology such as folding are found at the ponding stage of subduction; those are enhanced by weak slabs as well as reflective boundary conditions with small aspect ratios; both settings lead to a modulating effect of large scale convective cells on slab morphology. For large aspect ratios and periodic boundary conditions, this folding tendency of the slab is reduced.

Only periodic boundary condition models allows the excitation of a mean horizontal motion of the lower mantle with respect to the slab that corresponds to a net relative translation of the lower mantle. For the interpretation of horizontal velocities in such models it is then important to consider the physically appropriate reference frame (Garfunkel *et al.* 1986).

ACKNOWLEDGMENTS

We would like to thank two anonymous reviewers for their constructive and helpful comments.
TWB thanks Francesca Funiciello and Claudio Faccenna for discussions and was supported by the Cecil H. and Ida M. Green Foundation of IGPP, U.C. San Diego, and NSF grants EAR-0001046 and EAR-0112289.
This project was funded by the Deutsche Forschungsgemeinschaft (German Research Foundation).

REFERENCES

Becker, T. W. & Boschi, L., 2002. A comparison of tomographic and geodynamic mantle models, *Geochemistry, Geophysics, Geosystems*, **3**(2001GC000168).

Becker, T. W., Faccenna, C., O'Connell, R. J., & Giardini, D., 1999. The development of slabs in the upper mantle: insight from numerical and laboratory experiments, *J. Geophys. Res.*, **104**, 15207–15225.

Becker, T. W., Panasyuk, L. V., O'Connell, R. J., & Faccenna, C., 1999. The backward-bent Indonesia slab, *EOS Trans. AGU*, **80**, S18.

Bevis, M., 1988. Seismic slip and down dip strain rate in Wadati-Benioff zones, *Science*, **240**, 1317–1319.

Bevis, M., Taylor, F. W., Schutz, B. E., Recy, J., Isacks, B. L., Helu, S., Singh, R., Kendrick, E., Stowell, J., Taylor, B., & Calmant, S., 1995. Geodetic observations of very rapid convergence and back-arc extension at the Tonga arc, *Nature*, **374**, 249–251.

Bock, Y., Prawirodirdjo, L., Genrich, J. F., Stevens, C. W., McGaffrey, R., Subarya, C., Puntodewo, S. S. O., & Calais, E., 2003. Crustal motion in Indonesia from Global Positioning System measurements, *J. Geophys. Res.*, **108**, 2367, doi:10.1029/2001JB000324.

Byerlee, J., 1978. Friction of rock, *Pure Appl. Geophys.*, **116**, 615–626.

Christensen, U., 2001. Geodynamic models of deep subduction, *Phys. Earth Planet. Inter.*, **127**, 25–34.

Christensen, U. R., 1996. The influence of trench migration on slab penetration into the lower mantle, *Earth Planet. Sci. Lett.*, **140**, 27–39.

Čížková, H., van Hunen, J., van den Berg, A. P., & Vlaar, N. J., 2002. The influence of rheological weakening and yield stress on the interaction of slabs with the 670-km discontinuity, *Earth Planet. Sci. Lett.*, **199**, 447–457.

Conrad, C. P. & Hager, B. H., 1999. The effects of plate bending and fault strength at subduction zones on plate dynamics, *J. Geophys. Res.*, **104**, 17551–17571.

Davies, G. F., 1995. Penetration of plates and plumes through the mantle transition zone, *Earth Planet. Sci. Lett.*, **133**, 507–516.

Davies, G. F., 1999. *Dynamic earth: plate, plumes and mantle convection*, Press Syndicate of the University of Cambridge, Cambridge, 1st edn.

Faccenna, C., Becker, T. W., Lucente, F. P., Jolivet, L., & Rossetti, F., 2001. History of subduction and back-arc extension in the central Mediterranean, *Geophys. J. Int.*, **145**, 809–820.

Faccenna, C., Funiciello, F., Giardini, D., & Lucente, P., 2001. Episodic back-arc extension during restricted mantle convection in the Central Mediterranean, *Earth Planet. Sci. Lett.*, **187**,

105–116.

Faccenna, C., Bellahsen, N., Funiciello, F., Jolivet, L., & Piromallo, C., 2003. Remarks on the kinematics of the Tethyan slab, European Geosciences Union/American Geosciences Union/European Geophysical Society, 26th general assembly.

Faccenna, C., Jolivet, L., Piromallo, C., & Morelli, A., 2003. Subduction and the depth of convection in the Mediterranean mantle, *J. Geophys. Res.*, **108**(B2), 2099, doi:10.1029/2001JB001690.

Fukao, Y., Widiyantoro, S., & Obayashi, M., 2001. Stagnant slabs in the upper and lower mantle transition region, *Rev. Geophys.*, **39**, 291–323.

Funiciello, F., 2002. *Reconstruction of subduction processes in the Mediterranean by laboratory and numerical experiments*, Ph.D. thesis, Swiss Federal Institute of Technology, Zürich.

Funiciello, F., Faccenna, C., Giardini, D., & Regenauer-Lieb, K., 2003. Dynamics of retreating slabs: 2. Insights from three-dimensional laboratory experiments, *J. Geophys. Res.*, **108**, 2207, doi:10.1029/2001JB000896.

Funiciello, F., Morra, G., Regenauer-Lieb, K., & Giardini, D., 2003. Dynamics of retreating slabs: 1. Insights from two-dimensional numerical experiments, *J. Geophys. Res.*, **108**, 2206, doi:10.1029/2001JB000898.

Gaherty, J. B. & Hager, B. H., 1994. Compositional vs. thermal buoyancy and the evolution of subducted lithosphere, *Geophys. Res. Lett.*, **21**, 141–144.

Garfunkel, Z., Anderson, C. A., & Schubert, G., 1986. Mantle circulation and the lateral migration of subducted slabs, *J. Geophys. Res.*, **91**, 7205–7223.

Giardini, D. & Woodhouse, J. H., 1986. Horizontal shear flow in the mantle beneath the Tonga arc, *Nature*, **319**, 551–555.

Gottschaldt, K.-D., 1997. *Periodische Randbedingungen bei der zweidimensionalen numerischen Modellierung von Konvektion im Erdmantel*, Master's thesis, Friedrich-Schiller-Universität Jena, in german.

Gouillou-Frottier, L., Buttles, J., & Olson, P., 1995. Laboratory experiments on the structure of subducted lithosphere, *Earth Planet. Sci. Lett.*, **133**, 19–34.

Griffiths, R. W., Hackney, R. I., & van der Hilst, R. D., 1995. A laboratory investigation of effects

of trench migration on the descent of subducted slabs, *Earth Planet. Sci. Lett.*, **133**, 1–17.

Gurnis, M. & Hager, B. H., 1988. Controls of the structure of subducted slabs, *Nature*, **335**, 317–321.

Gurnis, M., Zhong, S., & Toth, J., 2000. On the competing roles of fault reactivation and brittle failure in generating plate tectonics from mantle convection, in *The History and Dynamics of Global Plate Motions*, edited by M. A. Richards, R. G. Gordon, & R. D. van der Hilst, vol. 121 of **Geophysical Monograph**, pp. 73–94, AGU, Washington DC.

Hager, B. H., 1984. Subducted slabs and the geoid: constraints on mantle rheology and flow, *J. Geophys. Res.*, **89**, 6003–6015.

Han, L. & Gurnis, M., 1999. How valid are dynamic models of subduction and convection when plate motions are prescribed?, *Phys. Earth Planet. Inter.*, **110**, 235–246.

Heidbach, O., 1999. *Der Mittelmeerraum. Numerische Modellierung der Lithosphärendynamik im Vergleich mit Ergebnissen aus der Satellitengeodäsie*, Ph.D. thesis, Ludwig-Maximilians-Universität München, in german.

Isacks, B. & Barazangi, M., 1977. Geometry of Benioff zones: lateral segmentations and downward bending of subducted lithosphere, in *Island arcs, Deep Sea Trenches, and Back-Arc Basins*, edited by M. Talwani & W. C. Pitman III, vol. 1 of **Maurice Ewing**, pp. 99–114, AGU, Washington DC.

Jarrard, R. D., 1986. Relations among subduction parameters, *Rev. Geophys.*, **24**, 217–284.

Kárason, H., 2002. *Constraints on mantle convection from seismic tomography and flow modeling*, Ph.D. thesis, Massachusetts Institute of Technology, Cambridge MA.

Kato, T., Kotake, Y., Nakao, S., Beavan, J., Hirahara, K., Okada, M., Hoshiba, M., Kamigaichi, O., Feir, R. B., Ho Park, P., Gerasimenko, M. D., & Kasahara, M., 1998. Initial results from WING, the continuous GPS network in the western Pacific area, *Geophys. Res. Lett.*, **25**, 369–372.

Kincaid, C. & Olson, P., 1987. An experimental study of subduction and slab migration, *J. Geophys. Res.*, **92**, 13832–13840.

King, S. D. & Hager, B. H., 1990. The relationship between plate velocity and trench viscosity

in Newtonian and power-law subduction calculations, *Geophys. Res. Lett.*, **17**, 2409–2412.

Letouzey, J., Werner, P., & Marty, A., 1990. Fault reactivation and structural inversion. Backarc and intraplate compressive deformations. Example of the eastern Sunda shelf (Indonesia), *Tectonophysics*, **183**, 341–362.

Lithgow-Bertelloni, C. & Richards, M. A., 1998. The dynamics of Cenozoic and Mesozoic plate motions, *Rev. Geophys.*, **36**, 27–78.

McClusky, S., Bassanian, S., Barka, A., Demir, C., Ergintav, S., Georgiev, I., Gurkan, O., Hamburger, M., Hurst, K., Kahle, H., Kastens, K., Kekelidze, G., King, R., Kotzev, V., Lenk, O., Mahmoud, S., Mishin, A., Nadariya, M., Ouzounis, A., Paradissis, D., Peter, Y., Preilepin, M., Reilinger, R., Sanli, I., Seeger, H., Tealeb, A., Toksoz, M. N., & Veis, G., 2000. Global Positioning System constraints on plate kinematics and dynamics in the eastern Mediterranean and Caucasus, *J. Geophys. Res.*, **105**, 5695–5719.

Mitrovica, J. X. & Forte, A. M., 1997. Radial profile of mantle viscosity: results from the joint inversion of convection and postglacial rebound observables, *J. Geophys. Res.*, **102**, 2751–2769.

Moresi, L. & Solomatov, V., 1998. Mantle convection with a brittle lithosphere: thoughts on the global tectonic styles of the Earth and Venus, *Geophys. J. Int.*, **133**, 669–682.

O'Connell, R. J., Gable, C. W., & Hager, B. H., 1991. Toroidal-poloidal partitioning of lithospheric plate motions, in *Glacial Isostasy, Sea-Level and Mantle Rheology*, edited by R. Sabadini, pp. 535–551, Kluwer Academic Publishers, Amsterdam.

Olbertz, D., Wortel, M., & Hansen, U., 1997. Trench migration and subduction zone geometry, *Geophys. Res. Lett.*, **24**, 221–224.

Piromallo, C. & Morelli, A., 2003. P wave tomography of the mantle under the Alpine-Mediterranean area, *J. Geophys. Res.*, **108**, 2065, doi:10.1029/2002JB001757.

Ranalli, G., 1995. *Rheology of the Earth*, Chapman & Hall, London, 2nd edn.

Ricard, Y., Doglioni, C., & Sabadini, R., 1991. Differential rotation between lithosphere and mantle: A consequence of lateral mantle viscosity variations, *J. Geophys. Res.*, **96**, 8407–8415.

Schmeling, H. & Marquart, G., 1991. The influence of second scale convection on the thickness of the continental lithosphere and crust, *Tectonophysics*, **189**, 281–306.

Schöffel, H.-J. & Das, S., 1999. Fine details of the Wadati-Benioff zone under Indonesia and its geodynamic implications, *J. Geophys. Res.*, **104**, 13101–13114.

Schott, B. & Schmeling, H., 1998. Delamination and detachment of a lithospheric root, *Tectonophysics*, **296**, 225–247.

Sella, G. F., Dixon, T. H., & Mao, A., 2002. REVEL: A model for Recent plate velocities from space geodesy, *J. Geophys. Res.*, **107**, 2081, doi:10.1029/2000JB000033.

Spakman, W., van der Lee, S., & van der Hilst, R., 1993. Travel-time tomography of the European-Mediterranean mantle down to 1400 km, *Phys. Earth Planet. Inter.*, **79**, 3–74.

Steinberger, B., 2000. Slabs in the lower mantle – results of dynamic modelling compared with tomographic images and the geoid, *Phys. Earth Planet. Inter.*, **118**, 241–257.

Steinberger, B. & O'Connell, R. J., 1998. Advection of plumes in mantle flow: implications for hotspot motion, mantle viscosity and plume distribution, *Geophys. J. Int.*, **132**, 412–434.

Tan, E., Gurnis, M., & Han, L., 2002. Slabs in the lower mantle and their modulation of plume formation, *Geochemistry, Geophysics, Geosystems*, **3**(2001GC000238).

Tao, W. C. & O'Connell, R. J., 1993. Deformation of a weak subducted slab and variation of seismicity with depth, *Nature*, **361**, 626–628.

Tetzlaff, M. & Schmeling, H., 2000. The influence of olivine metastability on deep subduction of oceanic lithosphere, *Phys. Earth Planet. Inter.*, **120**, 29–38.

Turcotte, D. & Schubert, G., 1982. *Geodynamics Application of continuum physics to geological problems*, John Wiley & Sons, New York.

van der Hilst, R. D., 1995. Complex morphology of subducted lithosphere in the mantle beneath the Tonga trench, *Nature*, **374**, 154–157.

Vassiliou, M. S. & Hager, B. H., 1988. Subduction zone earthquakes and stress in slabs, *Pure Appl. Geophys.*, **128**, 547–624.

Weidner, D. J. & Wang, Y., 1998. Chemical- and Clapeyron-induced buoyancy at the 660 km discontinuity, *J. Geophys. Res.*, **103**, 7431–7441.

Zhong, S., 2001. Role of ocean-continent contrast and continental keels on plate motion, net rotation of lithosphere, and the geoid, *J. Geophys. Res.*, **106**, 703–712.

Zhong, S. & Gurnis, M., 1994. Controls on trench topography from dynamic models of subducted slabs, *J. Geophys. Res.*, **99**, 15683–15695.

Zhong, S. & Gurnis, M., 1995. Mantle convection with plates and mobile, faulted plate margins, *Science*, **267**, 838–842.

Zhong, S. & Gurnis, M., 1995. Towards a realistic simulation of plate margins in mantle convection, *Geophys. Res. Lett.*, **22**, 981–984.

Table 1. Model parameters

quantity	*symbol*	*value (range)*	*source*
cohesion	b	60 MPa	Byerlee (1978) for $z < 40$ km
density contrast between slab and mantle	$\Delta\rho\vert_{\text{slab}}$	50 kg/m^3	
domain height		1320 km	
domain width		3960 km	
friction coefficient	a	0.6	Byerlee (1978) for $z < 40$ km
gravitational acceleration	g	10 m/s^2	
pore pressure factor	λ	$0.01 \ldots 1$	
thickness of the slab	d	$66 \ldots 99$ km	
viscosity of the mantle	$\eta_{\text{N}}^{\text{m}}$	$\eta_{\text{N}}^{\text{um}}$ for $z < 660$ km	
		$\eta_{\text{N}}^{\text{lm}} = 50\eta_{\text{N}}^{\text{um}}$ for $z \geq 660$ km	
viscosity of the slab	$\eta_{\text{N}}^{\text{slab}}$	$100 \ldots 500\eta_{\text{N}}^{\text{um}}$	
viscosity reference (upper mantle)	$\eta_{\text{N}}^{\text{um}}$	10^{20} Pa·s	

Figure 1. Initial distribution of tracers for a free slab model and periodic boundary conditions. We show every 8-th and 4-th tracer in horizontal and vertical direction, respectively. Contour lines denote stream-function isolines with selected annotated contours. Non-dimensional stream function values of 1 correspond to 10^{-5} m^2/s.

Figure 2. Snapshots of subduction for a fixed slab with reflective boundary conditions for pore pressure factors $\lambda = 0.01$ (a, at time, t, of $t = 2.32$ Myrs), $\lambda = 0.1$ (b, $t = 4.42$ Myrs), and $\lambda = 1$ (c, $t = 10.17$ Myrs). Thickness of slab is $d = 99$ km and $\eta_N^{\rm slab} = 100\eta_N^{\rm m}$. This plot is similar to Fig. 1 but only slab material tracers are shown. Inset figures in the upper right corners show $\lg(\eta/\eta_{\rm um})$ near the slab bending region. Dark color means low and light color high viscosity.

Figure 3. Maximum depth of slab, $z_{\rm slab}$, for the fixed slab models of Fig. 2 versus time, t, for pore pressure factors of $\lambda = 0.01$, $\lambda = 0.1$, and $\lambda = 1$.

Figure 4. Reference subduction models ($d = 99$ km, $\eta_N^{\rm slab} = 100\eta_N^{\rm m}$,) for free slab with periodic boundary conditions (BCs) (a), free slab with reflective BCs (b), and fixed slab with reflective BCs (c). For time-dependence of several variables, see Fig. 5. Models shown here and in Figs 6 and 8 have $\lambda = 0.1$.

Figure 5. Maximum depth of slab, $z_{\rm slab}$, and vertical velocity of the lowermost part of the slab, $v^z_{\rm slab}$, (a, defined as the maximum z coordinate of the deepest tracer in the lowermost part of the slab, velocity derived from the z curve), trench velocity, $v_{\rm t}$, (b, defined by 11 tracers at the trench on the top of the model box), mean horizontal motion of the lower mantle, $\langle v^h_{\rm lm}\rangle$, (c, defined as average horizontal velocity at the grid points in the lower mantle), and horizontal velocity of the oceanic plate at the surface, $v_{\rm p}$, (d, defined as average velocity at the grid points in the oceanic plate at the surface), against time. Lines indicate free slab, periodic BCs (dashed), free slab, reflective BCs (dotted), and fixed slab, reflective BCs (dot-dashed); compare with Figs 4(a), (b), and (c), respectively.

Figure 6. Stiff slab model ($d = 99$ km, $\eta_N^{\rm slab} = 500\eta_N^{\rm m}$) for free slab with periodic BCs (a), free slab with reflective BCs (b), and fixed slab with reflective BCs (c) as in Fig. 4. For time-dependence of several variables, see Fig. 7.

Figure 7. Stiff slab: Maximum depth of slab, $z_{\rm slab}$, and vertical velocity of the lowermost part of the slab, $v^z_{\rm slab}$, (a), trench velocity, $v_{\rm t}$, (b), mean horizontal motion of the lower mantle, $\langle v^h_{\rm lm}\rangle$, (c), and horizontal velocity of the oceanic plate at the surface, $v_{\rm p}$, (d), (as in Fig. 5) for the stiff slab model of Fig. 6.

Figure 8. Thin slab model ($d = 66$ km, $\eta_N^{slab} = 100\eta_N^m$) for free slab with periodic BCs (a), free slab with reflective BCs (b), and fixed slab with reflective BCs (c) as in Fig. 4. For time-dependence of several variables, see Fig. 9.

Figure 9. Thin slab: maximum depth of slab, z_{slab}, and vertical velocity of the lowermost part of the slab, v_{slab}^z, (a), trench velocity, v_t, (b), mean horizontal motion of the lower mantle, $\langle v_{lm}^h \rangle$, (c), and horizontal velocity of the oceanic plate at the surface, v_p, (e), (as in Fig. 5) for the thin slab model of Fig. 8.

Figure 10. Relative trench migration velocities for free periodic and reflective slabs.

Figure 11. Trench migration velocities with respect to the lower mantle (v_t^{lm}) and to the model box (v_t^b) for reference model free slab, periodic BCs, (a), and reference model free slab, reflective BCs, (b). Compare with box reference-frame rates shown in Fig. 5b.

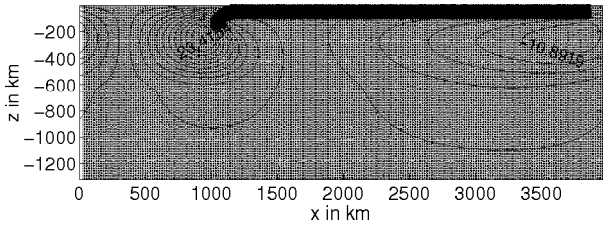
−200
−400
−600
−800
−1000
−1200
z in km
0
500
1000
1500
2000
2500
3000
3500
x in km

Figure 1

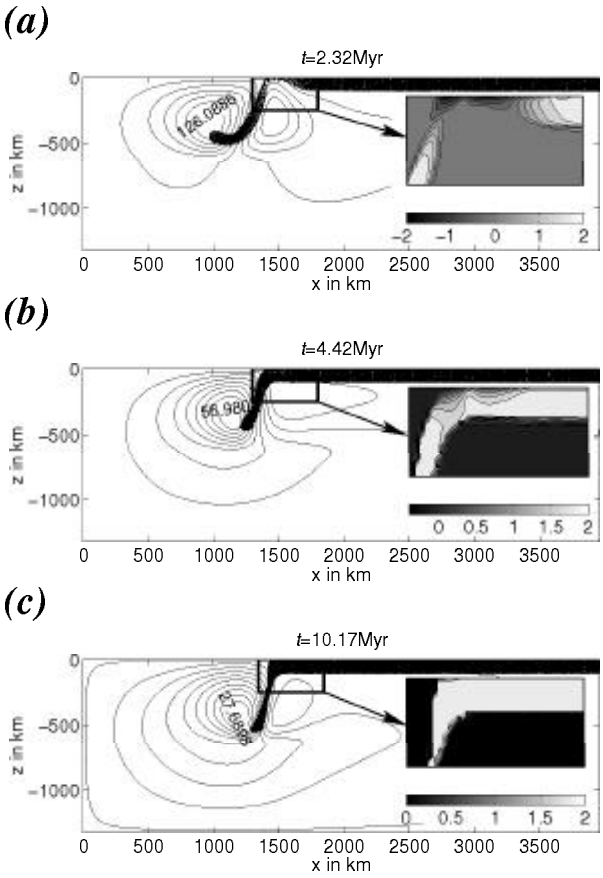
(a)
t=2.32Myr
126.0859
z in km
0
−500
−1000
−2 −1 0 1 2
0 500 1000 1500 2000 2500 3000 3500
x in km
(b)
t=4.42Myr
66.980
z in km
0
−500
−1000
0 0.5 1 1.5 2
0 500 1000 1500 2000 2500 3000 3500
x in km
(c)
t=10.17Myr
27.6898
z in km
0
−500
−1000
0 0.5 1 1.5 2
0 500 1000 1500 2000 2500 3000 3500
x in km

Figure 2

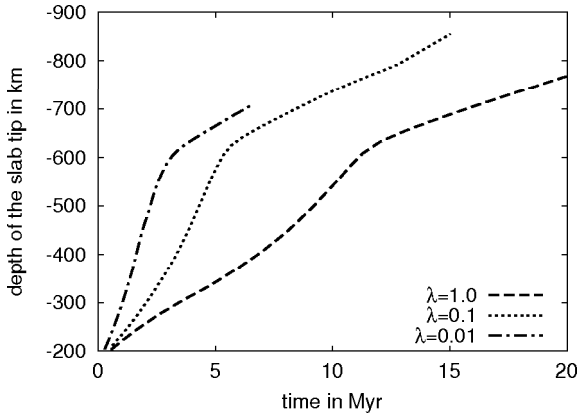
-900
-800
-700
-600
-500
-400
-300
-200
depth of the slab tip in km
0
5
10
15
20
time in Myr
λ=1.0
λ=0.1
λ=0.01

Figure 3

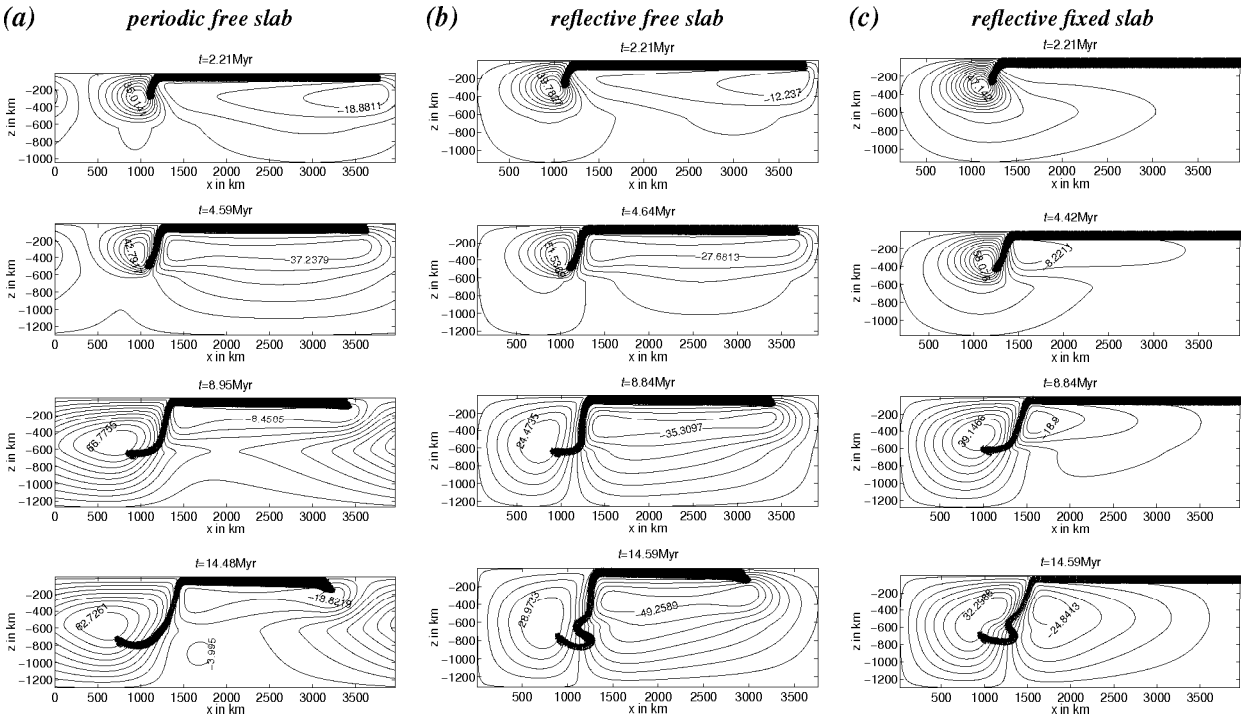
(a) periodic free slab
(b) reflective free slab
(c) reflective fixed slab
t=2.21Myr
t=4.59Myr
t=8.95Myr
t=14.48Myr
t=2.21Myr
t=4.64Myr
t=8.84Myr
t=14.59Myr
t=2.21Myr
t=4.42Myr
t=8.84Myr
t=14.59Myr
z in km
x in km

Figure 4

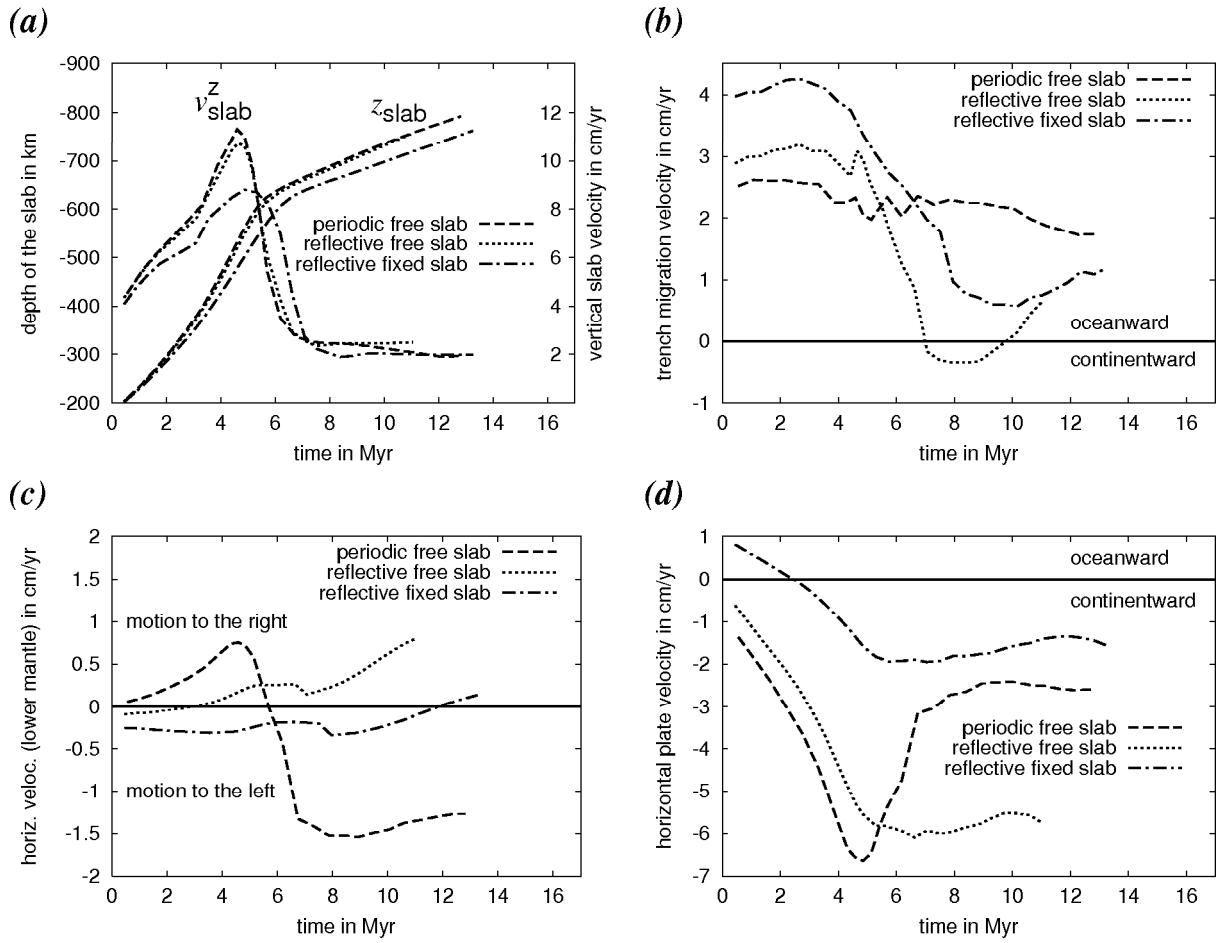
(a)
depth of the slab in km
vertical slab velocity in cm/yr
time in Myr
v^z_{slab}
z_{slab}
periodic free slab
reflective free slab
reflective fixed slab
(b)
trench migration velocity in cm/yr
time in Myr
oceanward
continentward
(c)
horiz. veloc. (lower mantle) in cm/yr
time in Myr
motion to the right
motion to the left
(d)
horizontal plate velocity in cm/yr
time in Myr
oceanward
continentward

Figure 5

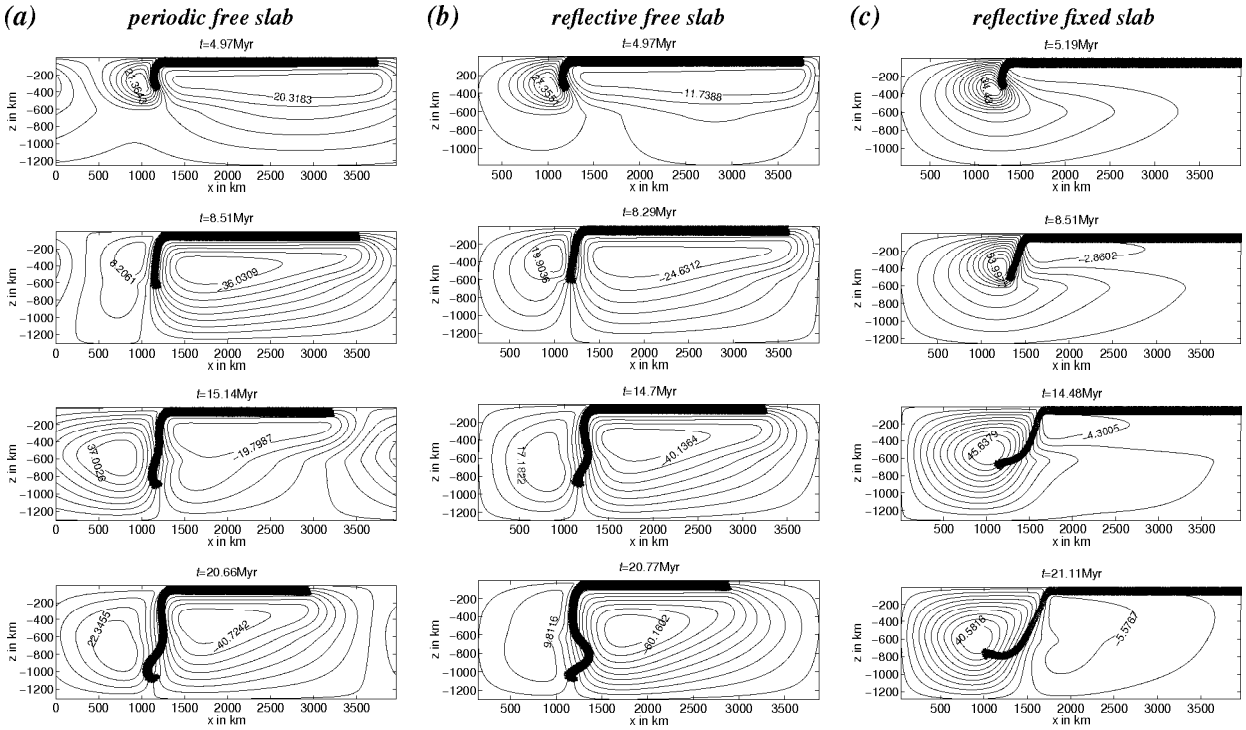
(a) periodic free slab
(b) reflective free slab
(c) reflective fixed slab
t=4.97Myr
t=4.97Myr
t=5.19Myr
t=8.51Myr
t=8.29Myr
t=8.51Myr
t=15.14Myr
t=14.7Myr
t=14.48Myr
t=20.66Myr
t=20.77Myr
t=21.11Myr
z in km
x in km

Figure 6

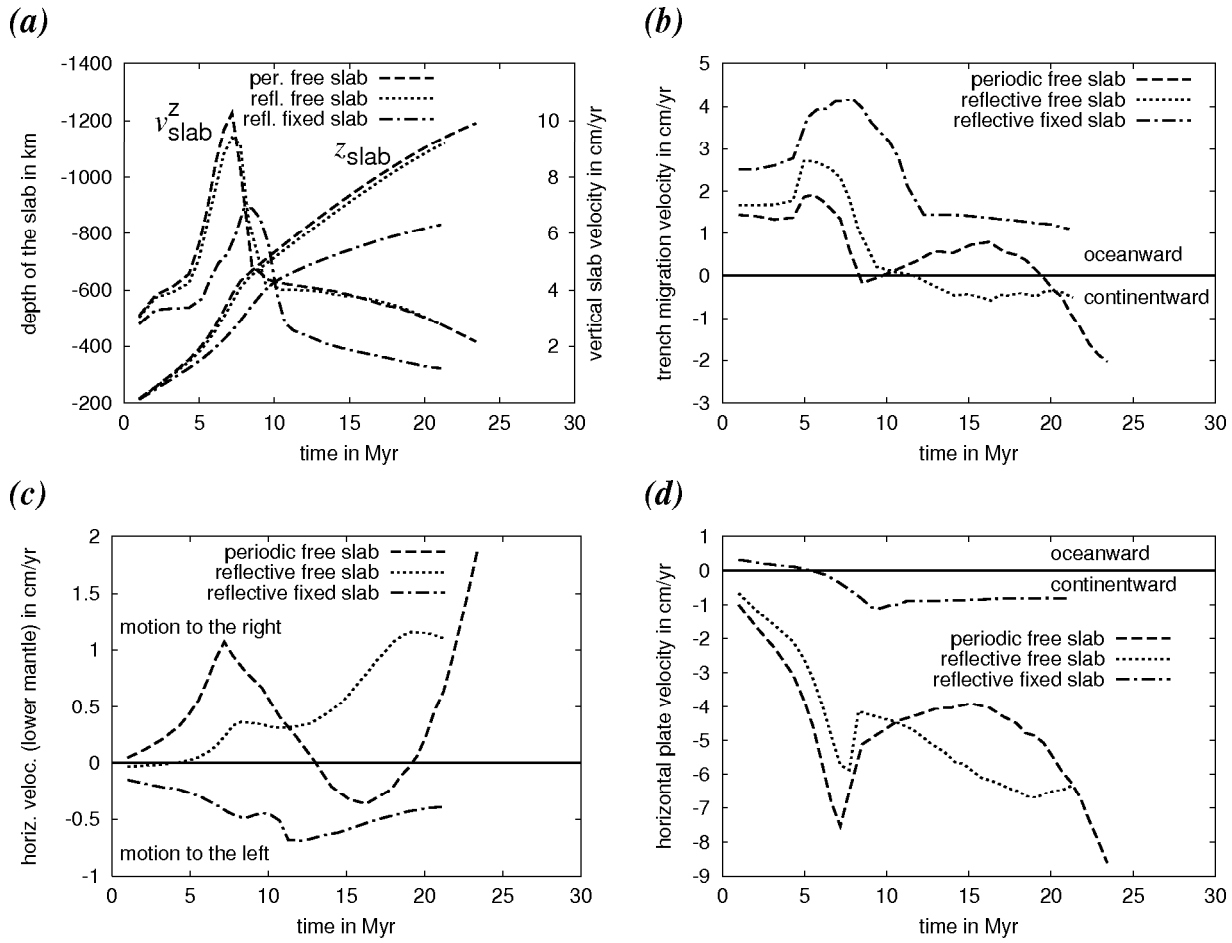
(a)
per. free slab
refl. free slab
refl. fixed slab
v^z_{slab}
z_{slab}
depth of the slab in km
vertical slab velocity in cm/yr
time in Myr
(b)
periodic free slab
reflective free slab
reflective fixed slab
oceanward
continentward
trench migration velocity in cm/yr
time in Myr
(c)
periodic free slab
reflective free slab
reflective fixed slab
motion to the right
motion to the left
horiz. veloc. (lower mantle) in cm/yr
time in Myr
(d)
oceanward
continentward
periodic free slab
reflective free slab
reflective fixed slab
horizontal plate velocity in cm/yr
time in Myr

Figure 7

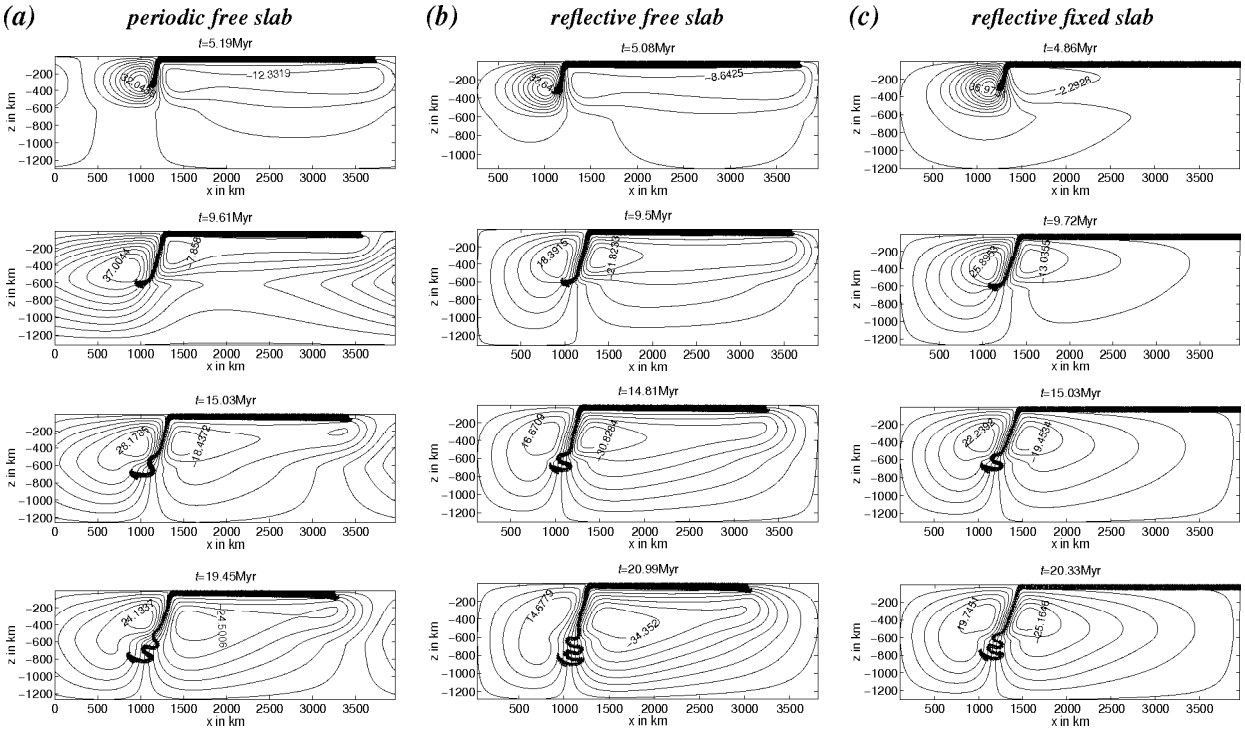
(a) periodic free slab
(b) reflective free slab
(c) reflective fixed slab
t=5.19Myr
t=5.08Myr
t=4.86Myr
t=9.61Myr
t=9.5Myr
t=9.72Myr
t=15.03Myr
t=14.81Myr
t=15.03Myr
t=19.45Myr
t=20.99Myr
t=20.33Myr
z in km
x in km

Figure 8

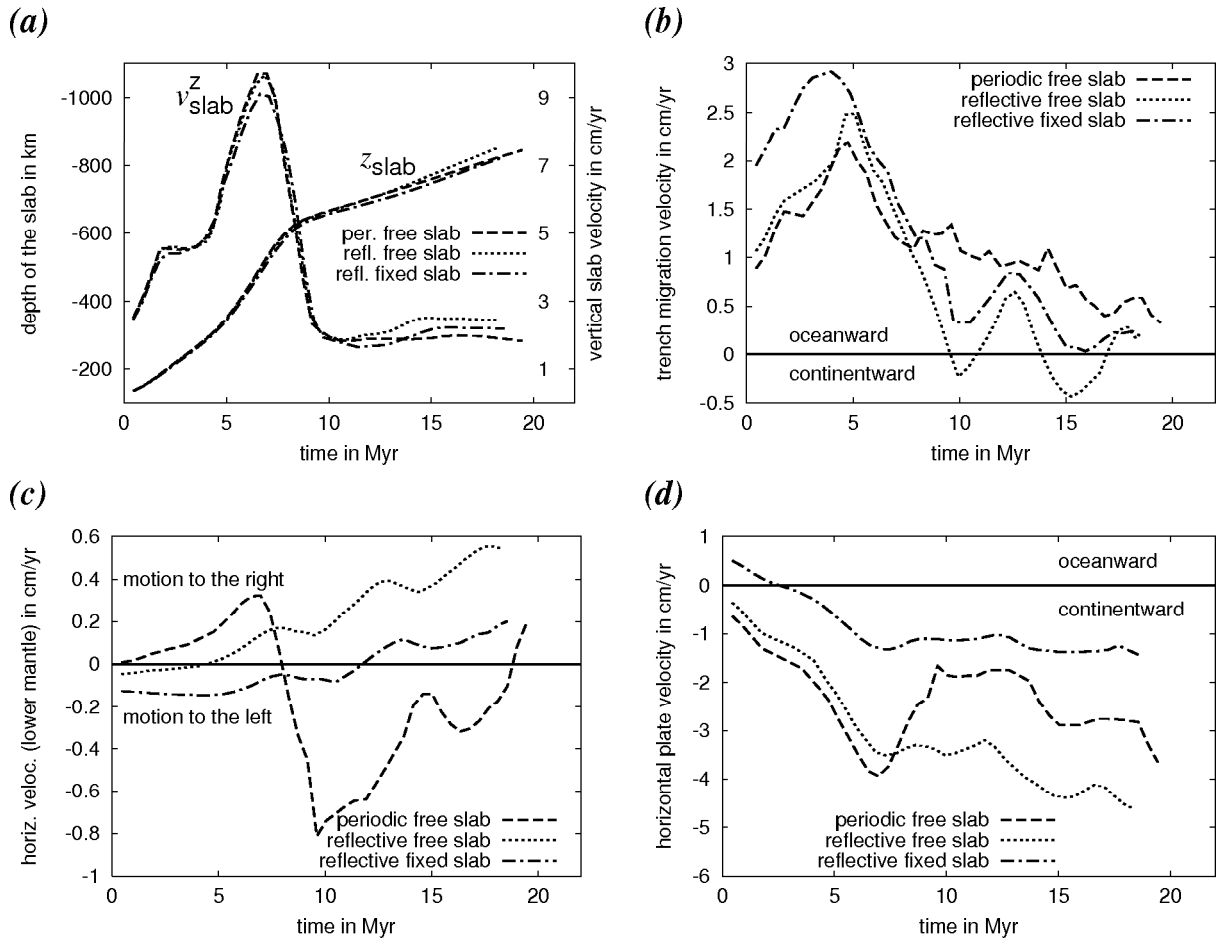
(a)
depth of the slab in km
vertical slab velocity in cm/yr
time in Myr
v^z_{slab}
z_{slab}
per. free slab
refl. free slab
refl. fixed slab
(b)
trench migration velocity in cm/yr
time in Myr
periodic free slab
reflective free slab
reflective fixed slab
oceanward
continentward
(c)
horiz. veloc. (lower mantle) in cm/yr
time in Myr
motion to the right
motion to the left
periodic free slab
reflective free slab
reflective fixed slab
(d)
horizontal plate velocity in cm/yr
time in Myr
oceanward
continentward
periodic free slab
reflective free slab
reflective fixed slab

Figure 9

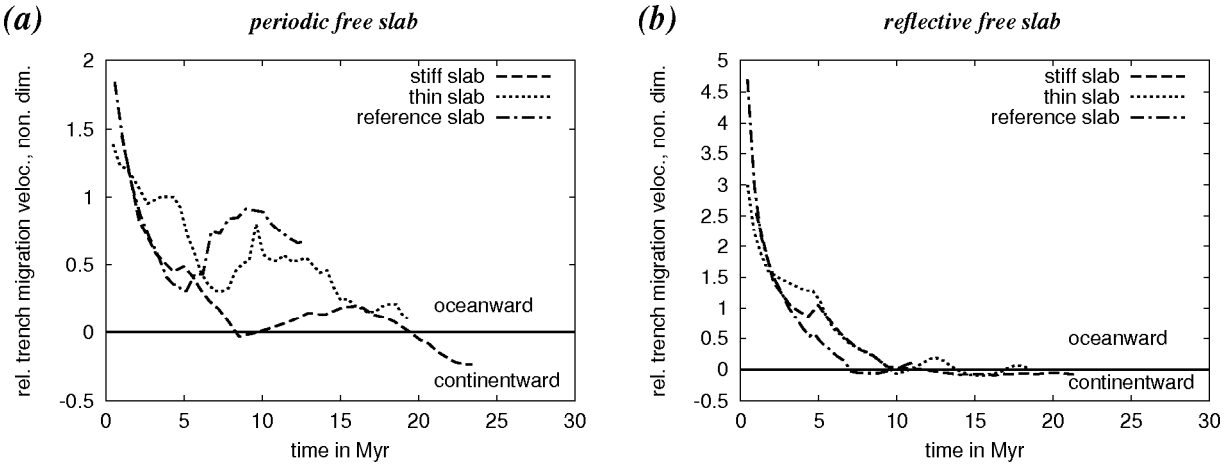
(a)
periodic free slab
rel. trench migration veloc., non. dim.
time in Myr
stiff slab
thin slab
reference slab
oceanward
continentward
(b)
reflective free slab
rel. trench migration veloc., non. dim.
time in Myr
stiff slab
thin slab
reference slab
oceanward
continentward

Figure 10

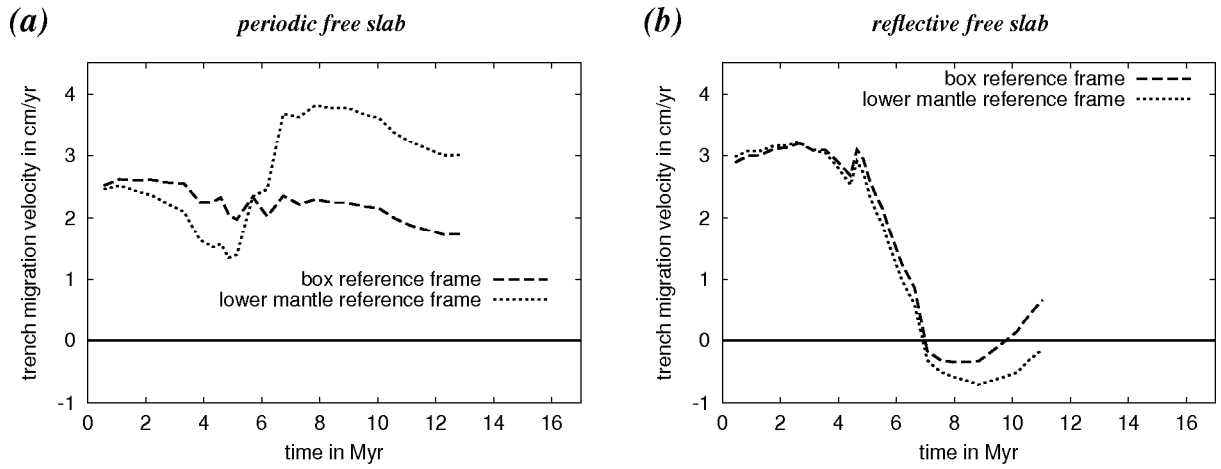
(a)
periodic free slab
trench migration velocity in cm/yr
time in Myr
box reference frame
lower mantle reference frame
(b)
reflective free slab
trench migration velocity in cm/yr
time in Myr
box reference frame
lower mantle reference frame

Figure 11